

© [2026 IEEE](#). Personal use of this material is permitted. Permission from IEEE must be obtained for all other uses, in any current or future media, including reprinting/republishing this material for advertising or promotional purposes, creating new collective works, for resale or redistribution to servers or lists, or reuse of any copyrighted component of this work in other works.

Digital Object Identifier (DOI): [10.1109/powertech59965.2025.11180299](https://doi.org/10.1109/powertech59965.2025.11180299)

2025 IEEE Kiel PowerTech

Inertia Evaluation in Grid-Forming Converters Using Time-Domain Modeling

Z. Zhou, S. Pugliese, M. Langwasser and M. Liserre

Suggested Citation

Z. Zhou, S. Pugliese, M. Langwasser and M. Liserre, "Inertia Evaluation in Grid-Forming Converters Using Time-Domain Modeling", 2025 IEEE Kiel PowerTech, 2025, DOI: [10.1109/powertech59965.2025.11180299](https://doi.org/10.1109/powertech59965.2025.11180299)

Inertia Evaluation in Grid-Forming Converters Using Time-Domain Modeling

Ziqi Zhou

*Chair of Power Electronics
Kiel University
Kiel, Germany
ziqi@tf.uni-kiel.de*

Sante Pugliese

*Chair of Power Electronics
Kiel University
Kiel, Germany
sapu@tf.uni-kiel.de*

Marius Langwasser

*Chair of Power Electronics
Kiel University
Kiel, Germany
mlan@tf.uni-kiel.de*

Marco Liserre

*Chair of Power Electronics
Kiel University
Kiel, Germany
ml@tf.uni-kiel.de*

Abstract—Grid-Forming (GFM) converters exhibit stability issues that worsen as the inertia coefficient increases. Novel power synchronization control methods have been proposed in the literature to improve GFM converters stability. Frequency-domain based inertia evaluation is typically used to adjust the control parameters of these methods, ensuring frequency responses align with the inertia and droop requirements outlined in the grid code. Therefore, the actual inertia performance of the converter highly depends on the accuracy of the inertia evaluation. In this paper, a straightforward inertia evaluation method using time-domain modeling is proposed. This method demonstrates that frequency-domain approaches can introduce errors, especially under high droop conditions. As a result, control parameters tuned using frequency-domain approaches may lead to a mismatch between the required inertia and the actual inertia, potentially violating the grid codes. In contrast, the proposed method helps in tuning the control parameters of GFM converter to achieve more accurate inertia behavior, ensuring grid codes compliance. Experimental and simulation results validate the effectiveness of the proposed method.

Index Terms—Inertia, droop, evaluation, grid-forming, frequency support, parameters tuning, frequency-domain modeling, time-domain modeling.

I. INTRODUCTION

The development of renewable energy is rapidly transforming the traditional power system, which is based on synchronous generators, into a power electronics-based system [1]. Such transition reduces the total inertia of the system as the rotating mass is gradually shifted out, decreasing the total stored kinetic energy of the power system. As a consequence, power system frequency stability problems have become more prominent and have received increased attention [2].

To enhance frequency stability in power systems with high penetration of power electronics, grid-forming (GFM) control in power converters has been developed to mimic the swing equation of a synchronous generator [2], [3]. In addition to enhancing frequency stability, further research has demonstrated that the integration of GFM converters can also contribute to sequence harmonic attenuation, sub-synchronous oscillation damping and grid voltage support, etc [4]–[7].

Along with the development of new control strategies for power converters, many countries are revising their grid codes to enhance the frequency regulation requirements for renewable energy sources, including wind power plants (WPPs).

Specifically, these codes require WPPs to provide inertia and droop responses under a frequency event [8].

To meet the inertia and droop requirements, a conventional GFM converter can be adjusted by tuning its inertia and droop coefficients in the active power control loop [9], [10]. However, high inertia requirements can lead to stability issues in the conventional GFM converter, especially under conditions of low droop requirements. To address this issue, one solution is to modify the structure of the GFM active power control loop [4], [11], [12]. This control strategy enhance system stability by either applying a lead-lag filter to the feedback loop or reconfiguring the swing equation.

Since these control strategies often change the transfer function of the GFM active power loop, the control parameters must be tuned to ensure that the power response complies with the inertia and droop requirements. In this context, accurate inertia evaluation of the converter should be prioritized. Frequency-domain modeling is commonly used for inertia evaluation, where the inertia of the converter is expressed as a function of the control parameters [11], [12]. Under the assumption that the evaluated inertia matches the actual inertia of the GFM converter, the required inertia specified by the grid codes can be achieved by tuning the control parameters to align the evaluated inertia with the required value.

In addition to frequency-domain modeling analysis, this paper proposes a time-domain-based inertia evaluation method. The proposed method reveals additional droop-related coupling terms that are hidden in the evaluated inertia function derived from frequency-domain modeling-based methods. These additional coupling terms indicate that frequency-domain modeling-based methods lead to inaccurate inertia evaluation under high droop conditions, resulting in a mismatch between the actual inertia and the required one. As a result, the actual inertia will be deviated from the required one. As stricter grid codes on power regulation accuracy are being introduced (e.g., the power regulation error must be lower than $0.01P_{nom}$ in China), inaccurate actual inertia resulting from incorrect inertia evaluation could lead to non-compliance with these grid codes [8]. Instead, the proposed method provides a simple way to evaluate the correct inertia of the GFM converter, allowing control parameters to be tuned accordingly to ensure the actual inertia complies with the grid codes.

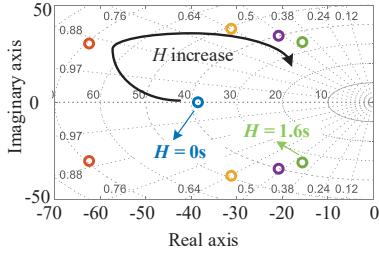


Fig. 4: Eigenvalues of GFM converter under various $J(H)$. ($k_{df} = 0.01$)

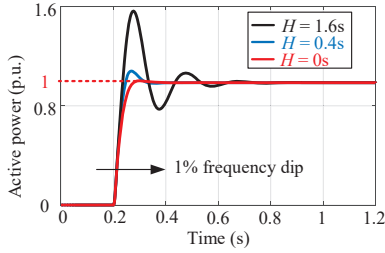


Fig. 5: GFM power response to 1% grid frequency drop under various $J(H)$. ($k_{df} = 0.01$)

on the real axis dominates the system dynamics, indicating an over-damped system. In this condition there is no overshoot in the transient of P_{GFM} during a step change of ω_g . As H increases, a pair of complex dominant eigenvalues emerge and shift toward the right half-plane, indicating a reduction in the damping ratio ξ . As ξ is also correlated with the overshoot ratio, increasing inertia leads to a worse dynamic of P_{GFM} under a ω_g step change.

The simulation results of P_{GFM} under ω_g step change are shown in Fig. 5. In the simulation, $L_2 = 0.6\text{mH}$, $L_g = 0.4\text{mH}$ and $P_{ref} = 125\text{kW}$. For the cases with $H = 0\text{s}$ and $H = 0.4\text{s}$, the GFM power shows good oscillation damping, while a weakly damped oscillation mode around 5Hz can be observed with $H = 1.6\text{s}$. Moreover, the GFM power with $H = 0.4\text{s}$ is always higher than that with $H = 0\text{s}$.

It can be concluded that increasing inertia coefficients leads to power overshoot during the transient phase of a frequency event and reduces system stability. Therefore, novel control strategy should be developed to damp the oscillation caused by high inertia while keeping the same frequency support behavior.

III. REVIEW OF TWO GFM CONTROL WITH FLEXIBLE DROOP AND INERTIA

This section introduces and reviews two state-of-the-art GFM control strategies that address the conflict between achieving high-inertia behavior and maintaining system stability [11], [12]. Each strategy is analyzed based on the approach

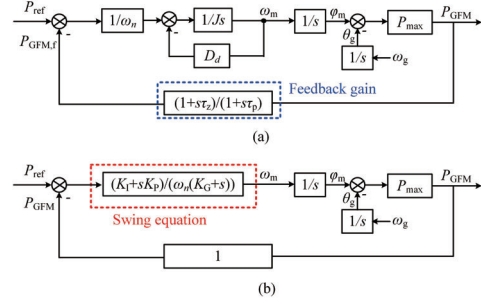


Fig. 6: Models of active power loop. (a) Lead-lag filter [11]. (b) Configurable natural droop [12].

used by the authors to evaluate inertia and droop in their control parameter design.

A. Introduction of GFM control strategies with flexible configuration of inertia and droop

Fig. 6. shows the active power loop models of two GFM controls which can realize flexible configuration of the equivalent inertia and droop [11], [12]. In Fig. 6(a), a lead-lag (LL) filter is applied in the feedback loop, while in Fig. 6(b), a configurable natural droop (CND) loop replaces the conventional swing equation. Based on this, parameter tuning methods for the stability improvement and required frequency support performance are given in the following parts.

B. Parameters design principles for the stability improvement

The LL based solution has a similar control structure of the conventional GFM control in Fig. 2. The difference is that the feedback gain of the active power loop is replaced by a lead-lag filter, expressed as:

$$G_{LL}(s) = (1 + s\tau_z)/(1 + s\tau_p). \quad (9)$$

With the additional lead-lag filter, the transfer function from the grid frequency to the GFM power $P_{GFM}(s)/\omega_g(s)$ can be rewritten as:

$$LL(s) = \frac{-\omega_n P_{max} (1 + s\tau_p) (D_d + Js)}{J\omega_n \tau_p s^3 + a_{LL2} s^2 + a_{LL1} s + P_{max}}, \quad (10)$$

where

$$a_{LL2} = \omega_n (J + D_d \tau_p), a_{LL1} = (\omega_n D_d + P_{max} \tau_z). \quad (11)$$

From (10) and (11), the introduction of lead-lag filter modifies the characteristic equation and the eigenvalues are changed as the consequence. Since low droop always leads to the worst stability condition, values of τ_z and τ_p are usually designed under $D_d=0$.

$$\tau_p = \sqrt{\frac{J\omega_n}{P_{max}(2\xi + 1)^3}}, \tau_z = \tau_p(2\xi + 1)^2. \quad (12)$$

The transfer function of the CND control can be expressed as:

$$G_{CND}(s) = \frac{K_I + K_P s}{\omega_n (K_G + s)}. \quad (13)$$

Similarly, the transfer function from the grid frequency to the GFM power $P_{GFM}(s)/\omega_g(s)$ can be rewritten as:

$$CND(s) = \frac{-\omega_n P_{max}(s + K_G)}{\omega_n s^2 + (\omega_n K_G + P_{max} K_P)s + P_{max} K_I}. \quad (14)$$

$$\xi = \frac{\omega_n K_G + P_{max} K_P}{2\omega_a \omega_n}. \quad (15)$$

$$\omega_a = \sqrt{\frac{P_{max} K_I}{\omega_n}}. \quad (16)$$

C. Frequency-domain modeling based droop evaluation

The droop power injection generally represent for the ratio between the power deviation and the grid frequency deviation under steady state [13]. Therefore, frequency-domain modeling based final value theorem is usually applied to calculate the droop coefficient of GFM control. According to (10) and (14), the equivalent droop coefficient of two methods can be calculated as:

$$D_{d,LL} = \lim_{s \rightarrow 0} -LL(s)/\omega_n = D_d, \quad (17)$$

$$D_{d,CND} = \lim_{s \rightarrow 0} -CND(s)/\omega_n = K_G/K_I, \quad (18)$$

where $D_{d,LL}$ and $D_{d,CND}$ are the evaluated droop coefficients of LL and CND methods derived from the frequency-domain modeling.

From (17) and (18), LL method keeps the original droop meaning of the conventional GFM control while CND method needs to tune its control parameters K_G and K_I for the required droop behavior.

D. Frequency-domain modeling based inertia evaluation

The inertia power injection is inversely proportional to the derivative of the grid frequency ω_g [14]. Similarly, the final value theorem can be also applied to analyze the inertia effect of a GFM converter:

$$J_{LL} = \lim_{s \rightarrow 0} -LL(s)/s\omega_n|_{D_d=0} = J, \quad (19)$$

where J_{LL} is the evaluated inertia coefficient of the LL method. Therefore, the LL method can also keep the original inertia meaning of the conventional GFM control.

The reason of setting $D_d = 0$ is to avoid infinite values of inertia [11]. As indicated from (17) - (19), the final value theorem always allows for obtaining a finite value for the droop coefficient, while a finite inertia coefficient can only be achieved under zero droop conditions. Therefore in [11], the equivalent inertia is designed first by setting $D_d = 0$. The value of D_d can then be configured based on the specific requirements. Under this condition, it was assumed that D_d has no effect on J_{LL} .

Another frequency-domain based inertia evaluation method was proposed in [12]. Here, the inertia coefficient is evaluated by equating (8) with (16) and it gives

$$J_{CND} = 1/K_I = J, \quad (20)$$

where J_{CND} is the evaluated inertia coefficient of the CND method. The reason for this equality is that both the CND

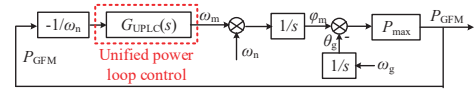


Fig. 7: Model of unified active power loop.

control and the conventional GFM control share a similar characteristic equation (see (6) and (14)). Since the system natural frequency ω_a in both methods is only affected by J and K_I , respectively, it is reasonable to consider that K_I has the equivalent meaning of the inertia.

In summary, the evaluated inertia of both LL method and CND method is related to the corresponding control parameters. Particularly, LL method keeps the original meaning of J and D_d , while the CND method requires adjusting K_G and K_I to achieve the desired inertia and droop. The correctness of inertia evaluation has been experimentally validated in [11], [12] under the conditions of high inertia and zero (negligible) droop. However, the accuracy of inertia evaluation under high droop still requires further discussion and validation.

IV. PROPOSED TIME-DOMAIN INERTIA EVALUATION METHOD

The inertia evaluation methods mentioned in Section III were generally considered able to realize the match between the required inertia and the actual inertia from the GFM converter. In this section, a time-domain based inertia evaluation method is proposed and it shows that the previous inertia evaluation methods may mismatch with the actual inertia when droop is not zero.

A. Introduction of the proposed time-domain inertia evaluation method

Considering $\Delta P_{ref}=0$ and the unified power loop control (UPLC) shown in Fig. 7, the transfer function $P_{GFM}(s)/\omega_g(s)$ can be written as:

$$\frac{\Delta P_{GFM}(s)}{\Delta \omega_g(s)} = -\frac{\omega_n(a_n s^n + \dots + a_0 s^0)}{b_n s^m + \dots + b_0 s^0}. \quad (21)$$

Accordingly, time-domain differential equation of (21) can be obtained as:

$$\frac{b_n d^m \Delta P_{GFM}}{\omega_n dt^m} + \dots + \frac{b_0 d^0 \Delta P_{GFM}}{\omega_n dt^0} = \frac{-a_n d^n \Delta \omega_g}{dt^n} + \dots + \frac{-a_0 d^0 \Delta \omega_g}{dt^0}. \quad (22)$$

Indicating with J_i and D_i the actual inertia and droop of the GFM converter implemented with the UPLC (G_{UPLC} in Fig. 7), the output power P_{GFM} can be expressed, when the grid frequency ω_g changes at a constant rate of change of frequency (RoCoF) ω_{rocof} as [15]:

$$-\frac{\Delta P_{GFM}}{\omega_n} = J_i \frac{d\Delta \omega_g}{dt} + D_i \Delta \omega_g = J_i \omega_{rocof} + D_i \Delta \omega_g. \quad (23)$$

Substituting (23) and $\omega_g = \omega_n + \omega_{rocof}t$ into (22), it results in:

$$-(b_1 D_i \omega_{rocof}) + \frac{b_0 \Delta P_{GFM}}{\omega_n} = -a_1 \omega_{rocof} - a_0 \Delta \omega_g. \quad (24)$$

After rearrangement, (24) can be written as:

$$-\frac{\Delta P_{GFM}}{\omega_n} = \frac{a_1 - b_1 D_i}{b_0} \omega_{rocof} + \frac{a_0}{b_0} \Delta \omega_g. \quad (25)$$

Equating (23) with (25), the equivalent inertia and droop coefficients of the $G_{UPLC}(s)$ control can be obtained as:

$$J_i = \frac{a_1 - b_1 D_i}{b_0}, \quad D_i = \frac{a_0}{b_0}. \quad (26)$$

According to (26), for any type of GFM control, where the relationship between P_{GFM} and ω_g can be expressed in the form of (22), the inertia and droop coefficients can be evaluated as shown in (26).

B. Inertia evaluation of three GFM control methods using the proposed method

Applying the proposed inertia evaluation method to (6), (10) and (14), the result is:

$$J_r = J - \frac{\omega_n D_d^2}{P_{max}} \neq J. \quad (27)$$

$$J_{LLr} = J + D_d(\tau_p - \tau_z) - \frac{\omega_n D_d^2}{P_{max}} \neq J. \quad (28)$$

$$J_{CNDr} = \frac{1 - D_{d,CND} K_P}{K_I} - \frac{\omega_n D_{d,CND}^2}{P_{max}} \neq \frac{1}{K_I}. \quad (29)$$

where J_r , J_{LLr} and J_{CNDr} are the evaluated inertia coefficients of the conventional, LL and CND methods, respectively, using the proposed time-domain modeling.

From (27) - (29), the evaluated inertia of three GFM control methods show the same fixed error $\frac{\omega_n D_d^2}{P_{max}}$, comparing to those evaluated through the frequency-domain modeling. Besides, the LL method and the CND method have an additional error $D_d(\tau_p - \tau_z)$ and $-\frac{D_{d,CND} K_P}{K_I}$, respectively. These errors are highly related to the droop coefficient. Therefore, the mismatch only occurs when droop is not zero. When the droop is zero, all the methods align their actual inertia with the required inertia.

With the increase of droop, the evaluated inertia becomes inaccurate, thus leading to a mismatch between the evaluated and the actual inertia. Under this condition, control parameters tuned according to the evaluated inertia will cause mismatch between the required inertia and the actual inertia.

C. Simulation validation

To validate the correctness of the proposed method, Fig. 8 shows the P_{GFM} of LL and CND methods under a constant $\omega_{RoCoF} = -4\text{rad/s}$ with one second duration. In the simulation, $L_2 = 0.6\text{mH}$, $L_g = 0.4\text{mH}$, $P_{nom} = 125\text{kW}$, $H=1.6\text{s}$ and $k_{df}=0.01$. Indeed, H should be higher in a realistic case; however, this value is chosen to make the effect of the coupling term more prominent. According to (2) and (3), $J=4$ and $D_d=125$; $\tau_z = 0.05$ and $\tau_p = 0.0055$ are designed for $\xi=1$ in

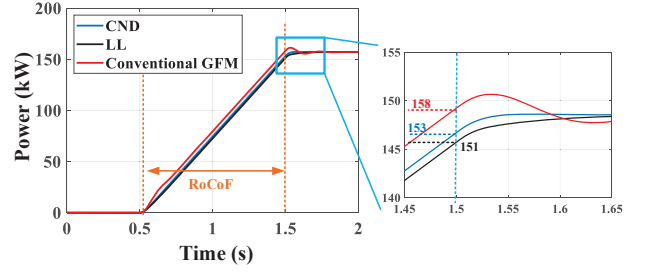


Fig. 8: GFM power response to -4rad/s RoCoF under various control strategy. ($k_{df} = 0.01$)

the lead-lag filter. For the CND method, with required $\xi=1$, $K_I=0.25$, $K_P=0.008$, and $K_G=31.25$. Moreover, the power response of the conventional GFM with $H=1.6\text{s}$ and $D_d=125$ is also given for comparison.

According to (27) - (29) and according to the given control parameters, the evaluated inertia of the three methods can be calculated as $J_r=0.7609$, $J_{CNDr}=-3.2391$ and $J_{LLr}=-4.8016$, respectively. Substituting (27) - (29) and $\omega_g = \omega_n + \omega_{rocof}(t - 0.5)$ into (23), the GFM power of conventional GFM, LL and CND methods at 1.5 second can be evaluated as $P_{r,conv}=158\text{kW}$, $P_{r,LL}=151\text{kW}$ and $P_{r,CND}=153\text{kW}$, respectively. The computed results matches well with the simulation results in Fig. 8, thus validating the correctness of the proposed inertia evaluation method. In addition, J_r , J_{CNDr} and J_{LLr} are negative, indicating a risk of deterioration in the frequency stability of the system.

It is worth noting that the evaluated GFM power of conventional GFM, LL and CND methods based on frequency-domain inertia evaluation method are all 162kW . It is evident that the frequency-domain inertia evaluation method significantly misrepresents the actual inertia behavior, leading to a mismatch between the evaluated and actual inertia.

Since the evaluated inertia is commonly considered equal to the required inertia, a function of power regulation error can be defined as:

$$PRG = \frac{P_{ev} - P_{act}}{P_{nom}}, \quad (30)$$

where P_{ev} and P_{act} are the evaluated (or required) power and the actual power, respectively.

Taking CND method as an example, with the frequency domain based inertia evaluation method, the power regulation error is calculated as $7.2\% > 1\%$, thus violating China grid codes [8]. With the proposed inertia evaluation method, the power regulation error is far smaller than 1% , which well complies with the grid codes. Therefore, the proposed inertia evaluation method helps in tuning the control parameters to match the actual inertia with the required inertia, and the power regulation error requirements can also be met. Similar conclusions can be obtained under the conditions of other active power control loops such as the LL method.

Since both LL and CND methods are developed to solve the stability issue of GFM converter at conditions of high inertia

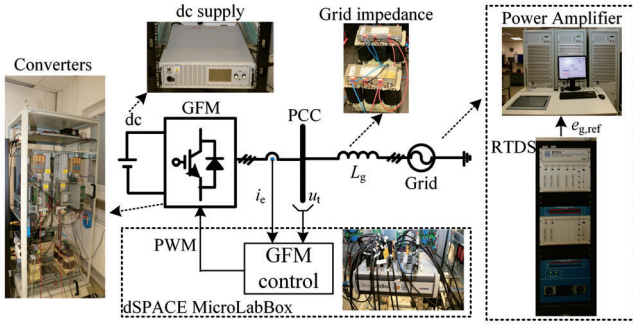


Fig. 9: Experiment setup.

and low droop. In these conditions, it is hard to notice the effect of droop on the actual inertia.

D. Sensitivity analysis

Taking CND method as an example, the partial derivative of (29) with respect to its droop coefficient is given by

$$\frac{\partial J_{CNDr}}{\partial D_{d,CND}} = \frac{-K_P}{K_I} - \frac{2\omega_n D_d}{P_{max}}. \quad (31)$$

From (31), it can be concluded that under fixed K_P and K_I , the incremental errors between the actual inertia and the evaluated (or the required) inertia become higher with the increase of droop or the decrease of the grid stiffness, i.e., a weaker grid. Similar conclusions can be derived for the other active power control loops.

E. Feasibility of online inertia evaluation

From Fig. 7, transfer function $P_{GFM}(s)/(-\omega_{ref}(s))$ can be written as:

$$\frac{\Delta P_{GFM}(s)}{-\Delta \omega_{ref}(s)} = -\frac{\omega_n(a_n s^n + \dots + a_0 s^0)}{b_n s^m + \dots + b_0 s^0}, \quad (32)$$

where ω_{ref} represents a tunable reference frequency within the GFM power control. Since (21) and (32) describe the same functional relationship, the online evaluation of system inertia becomes feasible by introducing a perturbation to ω_{ref} . This approach enables the indirect determination of the transfer function between P_{GFM} and ω_g , thereby facilitating the identification of the inertia-related coefficients outlined in (26).

V. EXPERIMENTAL RESULTS

In this section, the mismatch between the inertia evaluated by means of frequency-domain approaches and the actual inertia in different GFM implementations is experimentally validated in a micro-grid setup, shown in Fig. 9. In the setup, a power amplifier is used to emulate the power system to which its reference signal comes from a Real-Time Digital Simulator (RTDS). The power amplifier is then connected to the converter via series inductors that emulate the weak grid impedance. The dSPACE MicroLabBox is used for the control implementation. The converter platform contains two parallel converters, only one of which is used in the experiment. The

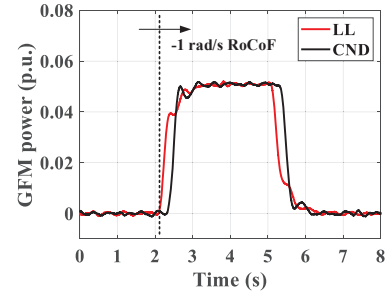


Fig. 10: GFM power under constant RoCoF.

TABLE I: Experiment Parameters

Symbol	Value	Symbol	Value	Symbol	Value
P_{nom}	1000W	Q_{ref}	0 Var	ω_n	314 rad/s
u_t	110 V	L_2	5 mH	R_s	4 Ω
L_g	25 mH	K	50	J	0.162
K_I	6.17	K_G	{0, 1.66, 3.32}	D_d	{0, 0.27, 0.54}
K_P	1.43	τ_z	0.31	τ_p	0.01

dc-link of the converter is powered by an external dc source. In addition, all the experimental results are filtered by a digital low-pass filter to mitigate the harmonic components.

The scaled system and controller parameters are listed in Table I. As this paper primarily investigates the impact of the droop coefficient on the system's inertia behavior, only the droop-related control parameters (such as K_G in the CND method and K_G in the LL method) are adjusted in the experiments, while all other parameters remain fixed. For the CND method, the gain values $K_G=\{0; 1.66; 3.32\}$ are selected, corresponding to droop coefficients $D_{d,CND}=\{0; 0.27; 0.54\}$, respectively. For the LL method, the same droop coefficients $D_d=\{0; 0.27; 0.54\}$ are chosen. With the parameters, the evaluated inertia under different methods can be obtained from (19), (20), (28) and (29), shown in Table II.

A. Frequency response of GFM converter under zero droop

As shown in Table II, all three methods yield identical inertia evaluation results under zero droop conditions. A constant RoCoF $\omega_{rocof} = -1$ rad/s is applied to the grid frequency ω_g to validate the accuracy of inertia evaluation. Based on this, the estimated power P_{ev} in the steady-state can be calculated as 0.05 p.u. according to equation (23), which is consistent with the experimental results in Fig. 10. This confirms that both the LL and CND methods accurately evaluate the inertia response when droop is zero. Under these conditions, the evaluated power P_{ev} equals the actual power P_{act} .

B. Frequency response of GFM converter with both inertia and droop

As the droop coefficient increases, only the proposed method accurately captures the influence of droop on the actual inertia coefficient. This effect leads to a mismatch between the power P_{ev} estimated by the LL and CND methods and the actual output power P_{act} . To verify the accuracy of inertia

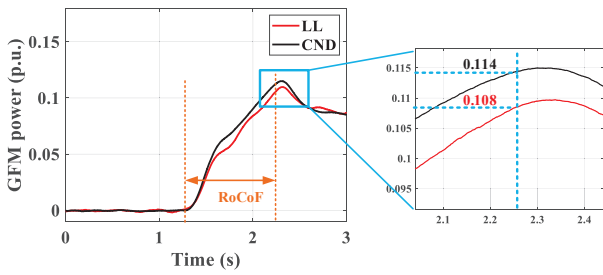


Fig. 11: Power response of GFM with droop $D_{d,1}=0.27$.

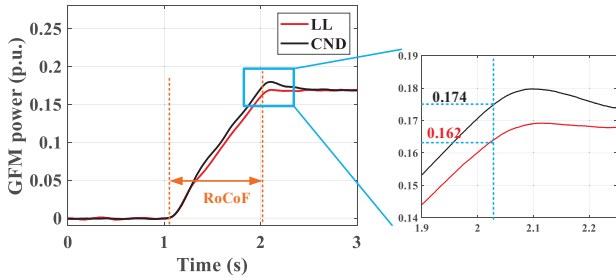


Fig. 12: Power response of GFM with droop $D_{d,2}=0.54$.

evaluation, the reference power P_{ref} for both methods is set to zero, and a constant RoCoF of $\omega_{\text{rocof}} = -1$ rad/s is applied to the grid frequency ω_g for a duration of one second.

Based on this configuration, Fig. 11 and Fig. 12 show the power responses of the GFM converter under droop coefficients of $D_{d,1}=0.27$ and $D_{d,2}=0.54$, respectively. Due to the droop effect, the GFM power output P_{GFM} continues to increase during the RoCoF period. Therefore, the instantaneous power at the end of the RoCoF is taken as the actual power P_{act} for comparison.

The estimated power P_{ev} for each method is calculated using equation (23), where J_i is replaced by the corresponding inertia value listed in Table II. The computed results are summarized in Table III. It is evident that the proposed method yields P_{ev} values that closely match P_{act} , demonstrating high evaluation accuracy. In contrast, the LL and CND methods show increasing deviation from P_{act} as the droop coefficient increases.

Consequently, control parameters designed based on inertia values from the LL or CND methods may result in discrepancies between the expected and actual inertia behaviors, potentially violating grid code requirements. For example, with the LL method at $D_d = 0.27$, the power regulation error, calculated using (30), is $2.8\% > 1\%$, thus exceeding the limit defined by China grid codes.

VI. CONCLUSIONS

Accurate inertia evaluation of GFM converters is essential for tuning control parameters to align actual inertia with the requirements specified by grid codes. However, conventional

TABLE II: Evaluated inertia coefficient J_{LL} , J_{LLr} , J_{CND} and J_{CNDr}

Method	Droop		
	0	0.27	0.54
eq.(19) - Method in [11] for LL	0.1621	0.1621	0.1621
eq.(28) - Proposed method for LL	0.1621	0.0751	-0.0236
eq.(20) - Method in [12] for CND	0.1621	0.1621	0.1621
eq.(29) - Proposed method for CND	0.1621	0.0939	0.0139

TABLE III: Estimated power P_{ev} (p.u.)

Method	Droop		
	0	0.27	0.54
Method in [11] for LL	0.05	0.136	0.221
Proposed method for LL	0.05	0.108	0.162
Method in [12] for CND	0.05	0.135	0.220
Proposed method for CND	0.05	0.114	0.174

frequency-domain-based methods may produce inaccurate results under high droop settings and weak grid conditions, leading to significant mismatches between the actual and expected inertia. This discrepancy can result in power regulation errors that exceed acceptable limits. For example, with a droop coefficient of $D_d = 0.27$ and a RoCoF of -1 rad/s, the LL method yields an inertia evaluation error of -0.09 , leading to a power regulation error of up to 2.8% , which surpasses the 1% threshold defined by China grid codes.

To overcome this limitation, a time-domain-based inertia evaluation method is developed that can accurately determine the actual inertia of GFM converters even under high droop conditions. With the proposed approach, both inertia evaluation and power estimation errors become negligible. This enables precise tuning of control parameters, ensuring compliance with both inertia and power regulation requirements.

Future work will extend this research by incorporating virtual impedance/admittance control into GFM systems and analyzing performance under diverse operating conditions such as grid voltage faults.

ACKNOWLEDGMENT

The research leading to these results was supported by Wingrid Project with funding from the European Union's Horizon 2020 research and innovation programme under the Marie Skłodowska-Curie grant agreement No 861398 and Interreg Deutschland-Danmark with funds from the European Regional Development Fund via the Smart Power Conversion project (ref. 16-2.1-22 1). The authors gratefully acknowledge funding by the German Federal Ministry of Research, Technology and Space (BMFTR) within the Kopernikus Project ENSURE III 'New ENergy grid StructURes for the German Energiewende' (FKZ: 03SFK110-3).

REFERENCES

- [1] M. Liserre, M. A. Perez, M. Langwasser, C. A. Rojas, and Z. Zhou, "Unlocking the hidden capacity of the electrical grid through smart transformer and smart transmission," *Proceedings of the IEEE*, vol. 111, no. 4, pp. 421–437, 2023.
- [2] R. H. Lasseter, Z. Chen, and D. Pattabiraman, "Grid-forming inverters: A critical asset for the power grid," *IEEE Journal of Emerging and Selected Topics in Power Electronics*, vol. 8, no. 2, pp. 925–935, 2020.

- [3] Q.-C. Zhong and G. Weiss, "Synchronverters: Inverters that mimic synchronous generators," *IEEE Transactions on Industrial Electronics*, vol. 58, no. 4, pp. 1259–1267, 2011.
- [4] Z. Zhou, S. Pugliese, M. Langwasser, and M. Liserre, "Subsynchronous damping by battery storage system in grid-forming control," *IEEE Transactions on Power Electronics*, vol. 39, no. 4, pp. 4173–4186, 2024.
- [5] F. Mandrile, E. Carpaneto, and R. Bojoi, "Grid-feeding inverter with simplified virtual synchronous compensator providing grid services and grid support," *IEEE Transactions on Industry Applications*, vol. 57, no. 1, pp. 559–569, 2021.
- [6] R. Rosso, S. Engelken, and M. Liserre, "On the implementation of an firt strategy for grid-forming converters under symmetrical and asymmetrical grid faults," *IEEE Transactions on Industry Applications*, vol. 57, no. 5, pp. 4385–4397, 2021.
- [7] G. N. Baltas, N. B. Lai, L. Marin, A. Tarrasó, and P. Rodriguez, "Grid-forming power converters tuned through artificial intelligence to damp subsynchronous interactions in electrical grids," *IEEE Access*, vol. 8, pp. 93369–93379, 2020.
- [8] L. Li, D. Zhu, X. Zou, J. Hu, Y. Kang, and J. M. Guerrero, "Review of frequency regulation requirements for wind power plants in international grid codes," *Renewable and Sustainable Energy Reviews*, vol. 187, p. 113731, 2023.
- [9] P. Kundur, N. Balu, and M. Lauby, *Power System Stability and Control*. EPRI power system engineering series, McGraw-Hill, 1994.
- [10] Z. Zhou, S. Pugliese, and M. Liserre, "Stability comparison of grid-forming converters with different power calculation strategies," in *2023 IEEE 14th International Symposium on Power Electronics for Distributed Generation Systems (PEDG)*, pp. 800–805, 2023.
- [11] F. Mandrile, V. Mallemaçi, E. Carpaneto, and R. Bojoi, "Lead-lag filter-based damping of virtual synchronous machines," *IEEE Transactions on Industry Applications*, vol. 59, no. 6, pp. 6900–6913, 2023.
- [12] W. Zhang, A. M. Cantarellas, J. Rocabert, A. Luna, and P. Rodriguez, "Synchronous power controller with flexible droop characteristics for renewable power generation systems," *IEEE Transactions on Sustainable Energy*, vol. 7, no. 4, pp. 1572–1582, 2016.
- [13] R. Liu, C. Xue, and Y. R. Li, "Parameter feasible region construction of generalized virtual synchronous generators with improved damping capability," in *2023 11th International Conference on Power Electronics and ECCE Asia (ICPE 2023 - ECCE Asia)*, pp. 425–432, 2023.
- [14] M. Shadoul, R. Ahshan, R. S. AlAbri, A. Al-Badi, M. Albadi, and M. Jamil, "A comprehensive review on a virtual-synchronous generator: Topologies, control orders and techniques, energy storages, and applications," *Energies*, vol. 15, no. 22, p. 8406, 2022.
- [15] R. Eriksson, N. Modig, and K. Elkington, "Synthetic inertia versus fast frequency response: a definition," *IET renewable power generation*, vol. 12, no. 5, pp. 507–514, 2018.